ADVANCED MATERIALS TECHNOLOGIES
www.advmattechnol.de

Toward "Green" Vessels: Characterization of Microstructure, Mechanics, and Endothelial Cell Interaction on Three Macro-Tubular Plants for Vascular Tissue Engineering Applications

Ali Salehi, Meriem Ernez, Gemma Lucas Salido, and Giorgio Cattaneo*

Vascular tissue engineering aims to create vessel models for in vitro research and develop vascular grafts for in vivo applications using tubular scaffolds. Natural scaffolds outperform synthetic ones due to their biocompatibility and natural microenvironment supporting cell growth. Given the importance of producing biocompatible tubular scaffolds through cost-effective and uncomplicated processes, this study introduces nature-derived tubular structures from three decellularized tubular plants (Water Spinach, Green Onion, and Water Horsetail) as novel alternatives. Microstructural characterization on the luminal surfaces of the plants reveals unique surface topography for each. Water Spinach is the most promising graft candidate in suturability tests besides presenting the highest elongation before rupture in tensile test. Assessment of human endothelial cells on the luminal surfaces of decellularized scaffolds shows higher expression of Ki-67 protein and a consistent increase in cell number on water spinach and green onion scaffolds compared to tissue culture plate as a control. Focal adhesion-related molecule Vinculin is expressed more than twice on all scaffolds compared to control, and confluent cell monolayers are formed on water spinach and green onion scaffolds, as confirmed by VE-cadherin. This study proposes an innovative approach to use the natural structure of macro-tubular plants for the preparation of vascular scaffolds.

1. Introduction

Vascular tissue engineering aims at the dimensional and functional in vitro reproduction of blood vessels embedding human cells within synthetic or natural scaffolds. The resulting biologized scaffolds show a high potential for implantation as vascular grafts and models for in vitro research on cardiovascular diseases (CVD) and their treatment.

Vascular grafts are used to bypass or replace narrowed or occluded vessels through a surgical procedure. Synthetic vascular grafts made of Polyester[1] or expanded Polytetrafluoroethylene (PTFE)[2] as well as biological vascular grafts such as xenografts,[3] cryopreserved allografts[4] and human autologous grafts[5] have been used widely in patients. However, limitations such as poor long-term patency in small-diameter (<6 mm) as well as immune rejection and risk of animal-transmitted diseases in biological grafts remain a major concern.[6–8] Employing animal tissues in regenerative medicine offers advantages stemming from structural and organ similarities between animals and humans. However, this practice raises concerns regarding availability, reproducibility, high cost, and ethical considerations.[9,10] As an alternative, different approaches including electrospinning,[11,12] melt electrowriting,[13,14] casting,[15] rolling,[16] and 3D printing,[16,17] have been used to manufacture tubular scaffolds for the preparation of biologized vessel grafts. High cost of production, expensive equipment, complex process, possible production of toxic residues and byproducts are the reported drawbacks of these methods.[18] Vascular grafts must endure suture tension during implantation without rupturing, ensuring durability at the edges and the ability to withstand blood pressure.[19] Common methods for assessing the suitability of vascular grafts include testing suture retention strength and manually evaluating suturability.[20–23]

Vascular models are widely used to investigate catheter-based vascular implants such as stents, stent-grafts, or flow diverters intended for treatment of vascular diseases such as stenoses and aneurysms.[24] Preclinical tests aim to predict mechanical and other interactions between the implant and the surrounding tissue as well as the blood response to the foreign material, ensuring maximum safety. Generally, silicon or PVC tubes or block models with simplified anatomical characteristics are used to

A. Salehi, M. Ernez, G. L. Salido, G. Cattaneo
Institute of Biomedical Engineering
University of Stuttgart
Stuttgart, Germany
E-mail: ali.salehi@bmt.uni-stuttgart.de

The ORCID identification number(s) for the author(s) of this article can be found under https://doi.org/10.1002/admt.202401129

DOI: 10.1002/admt.202401129

investigate fluid dynamics[25–27] or blood reaction to foreign implant surfaces.[28,29] Vascular models including an endothelial cell layer have been presented with the aim of replicating the biological environment of a vascular implant,[30–34] potentially adding a biological component crucial for the investigation of implant-triggered thrombus formation and implant surface endothelialization. In fact, the endothelium lining of the native vasculature is resistant to thrombosis and regulates vessel function, platelet activation, and leukocyte adhesion.[35] As a result, the lack of endothelial cell monolayer on biomaterials used as vascular models favors thrombosis and thus distorts results in studies focusing on implant-blood interaction.[36] For this reason, the inclusion of an endothelial monolayer, known as endothelialization, on the luminal surface of vascular models has been investigated in some previous studies. However, after endothelialization of tubular scaffolds via a bioreactor, asymmetric cell adhesion as well as random cell orientation have been reported as drawbacks.[37–39] Moreover, stent implantation within previously endothelialized vascular models produced a detachment of endothelial cells.[37,38,40] Generation of surface topographies mimicking the natural cell environment by means of roughness, microchannels, nanofibers and microgrooves improved cell behavior in terms of proliferation and orientation in previous studies on planar substrates.[41–44]

Considering the limitations of current technologies, the importance of investigating novel materials and technologies for tubular scaffold fabrication and endothelialization appears to be extremely significant. Among them, decellularized tissues from natural sources have the potential to provide natural structures "designed" to host human cells. While animal tissues offer the advantage of human-similarity in mechanical and anatomical characteristics, concerns include low reproducibility, limited accessibility and availability, difficulties in extracting target tissues without damage and finally ethical issues.[45–48] Furthermore, α -gal carbohydrate antigen and major histocompatibility complex (MHC) molecules found in animal cell membranes represent the main cause of immune rejection during transplantation of decellularized animal scaffolds.[49]

Plant-based tissue engineering has the potential to play a significant role in the production of natural vascular grafts as well as models for in vitro cardiovascular research in the future. The structural framework of plant cell walls consists of polysaccharides including cellulose, hemicellulose, and pectin, alongside an assortment of proteins.[50] These polysaccharides contribute to structural integrity, mechanical strength, and flexibility.[51] Plant cells are made up of cellulose, a linear polymer organized into microfibrils. Cellulose, the most prevalent polysaccharide in nature, comprises linear chains consisting of β (1→4) D-glucose units. Cellulose is valued in biomedical research for its numerous advantageous properties, such as its widespread availability, biocompatibility, minimal cytotoxicity, biodegradability, and adjustable mechanical characteristics.[52] Cellulose finds applications in various areas of tissue engineering research and is also utilized in FDA-approved surgical wound dressings designed for hemostatic purposes and a commercial scaffold for the treatment of knee cartilaginous damages.[53,54] In recent times, cellulose has attracted attention for biomedical purposes like manufacturing hemodialysis membranes and vascular grafts due to the hemocompatibility, mechanical resilience, and flexibility of this material.[55,56]

The potential of plant-based cellulose scaffolds for cultivating mammalian cells in a 3D environment was first introduced by Modulevsky et al. where a decellularized apple scaffold provided an alternative method to current techniques.[57] This emerging path has been followed in more specific applications such as vascular, bone, cartilage, and skin tissue engineering, muscle regeneration, and drug delivery.[50,58–66] Notably, the available natural microenvironment in decellularized plant scaffolds promotes cell adhesion, proliferation, and differentiation.[50,62,67–73] Regarding surface modification of plant scaffolds, collagen coating, a well-known surface modification technique for decellularized plant scaffolds, has been frequently reported to enhance cell adhesion on these scaffolds.[57,61,66,74–79] Recent studies demonstrate in vitro and in vivo biocompatibility of plant-derived cellulose scaffolds.[50,75,80] Among others, a typical foreign body reaction to implanted decellularized apple scaffold in mice skin after 1 week and the disappearance of this immune response after 8 weeks has been reported.[80]

Although previous studies revealed the potential of decellularized plant tissues for several tissue engineering applications, a few studies investigated the potential of tubular plants for vascular tissue engineering. For instance, decellularized Parsley stems were recently introduced as potential vascular grafts, however, the narrow luminal dimension of this plant limits their application.[58] Given the importance of advancing vascular tissue engineering to overcome the limitations of existing vascular grafts and vessel models, this study aims to introduce innovative biologized tubular scaffolds derived from plants as a new approach. Among various plant options, three tubular plants with stable structures and large inner diameters ranging from 3.4 to 6.5 mm, referred to as "macro-tubular," were selected. These plants were decellularized and their luminal surfaces were examined using scanning electron microscopy (SEM) and confocal microscopy, followed by tensile testing to assess their mechanical properties. To evaluate the potential of decellularized plants as vascular grafts, their suturability was assessed by measuring suture retention strength and grafting onto animal coronary and pulmonary arteries. Endothelial cells were then cultured on the luminal surfaces of the plant-derived scaffolds. Finally, cell adhesion, proliferation, viability, and the formation of cell-to-cell and cell-to-substrate junctions were analyzed using fluorescence microscopy.

2. Results

2.1. Scaffold Characterization

2.1.1. Dimensional Characterization and DNA Quantification

Green onion (GO), Water spinach (WS) and Water horsetail (WH) plants were prepared for this study as can be seen respectively from left to right in **Figure 1**A. After the decellularization treatment, all plants lost their color while keeping their integrity (Figure 1B). Cross-sectional imaging (**Figure 2**) demonstrated that the tubular geometry of the plants was preserved after decellularization (D) treatment, comparable to that of the native plants

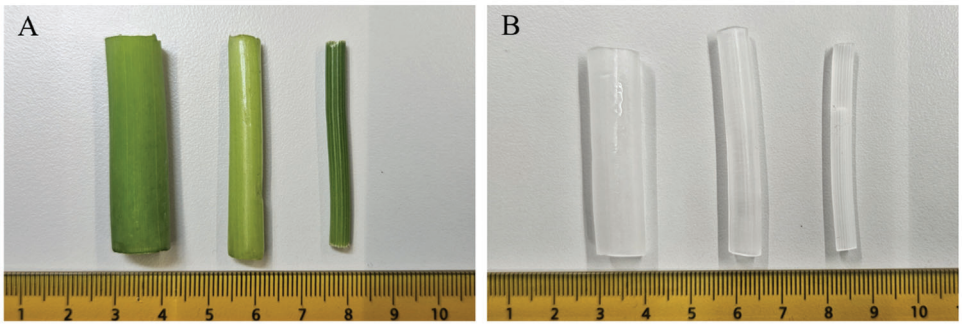

Figure 1. A) GO, WS, and WH plants in native and B) decellularized state.

(N). However, some inhomogeneity in the wall thickness of the decellularized plants was observed. The inner diameter and wall thickness were measured 6.61 ± 0.73 mm and 0.59 ± 0.16 mm for GO, 4.91 ± 0.34 mm and 1.10 ± 0.17 mm for WS and 3.40 ± 0.25 mm and 0.56 ± 0.13 mm for WH, respectively. Furthermore, the inner diameter and wall thickness variations in individual samples of each plant are presented in detail in, Table S2 (Supporting Information). DNA amount decreased significantly to less than 50 ng mg^{-1} tissue in all the decellularized plants (**Figure 3**).

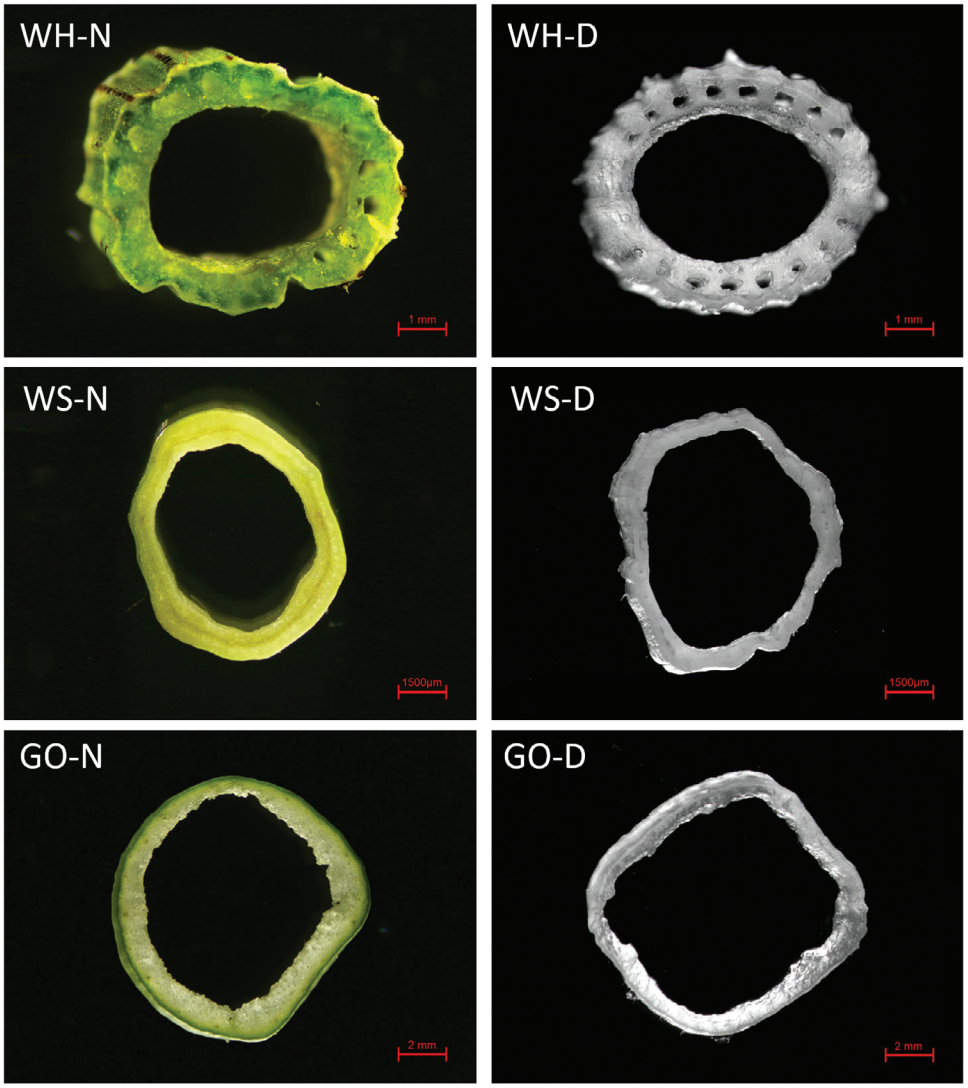

Figure 2. Cross-sectional microscopy of the plants before and after decellularization.

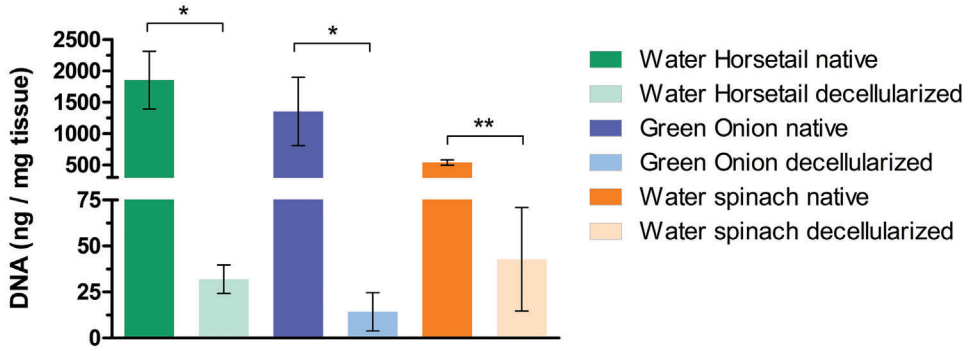

Figure 3. Detected DNA content in the native and decellularized plants ($n = 3$).

2.1.2. Microstructural Investigation

The microstructure of the scaffolds was evaluated by imaging from the inner surface of the tubular plants. Scanning electron microscopy (SEM) and confocal microscopy were utilized for morphological study of the scaffolds and the results are presented in **Figure 4**. Consistent results of SEM and confocal microscopy illustrate that plants' natural microstructures were only accessible after the decellularization treatment (Figure 4B,F,J) while covered before decellularization (Figure 4A,E,I). Accordingly, decellularization caused a rise in surface roughness for all plants. Microscopical data of decellularized WH demonstrated deep parallel grooves with a depth of 35.80 ± 1.47 µm and regular peaks and valleys formed longitudinally along the plant's inner surface (Figure 4J,L). Decellularized GO (Figure 4B,D) showed regular and rectangular depressions arranged on its surface, and areas with regular microstructures were observed on WS (Figure 4F,H). Microstructures were shallower in GO and WS compared to WH, amounting to ≈1.78 ± 0.32 and 3.26 ± 0.23 µm respectively. **Table 1** presents the microstructural characteristics of the samples.

2.1.3. Mechanical Characteristics

A tensile test was performed to determine Young´s modulus, tensile strength, and maximum elongation of the plant scaffolds. In general, decellularized tissues showed noticeably lower Young´s modulus, tensile strength, and maximum elongation compared to the native plants. As depicted in **Figure 5**A, native and decellularized WH showed the highest Young's module of 343.7 ± 15.6 and 73.9 ± 15.69 MPa respectively, and thus in higher order on magnitude compared to native and decellularized WS (21.54 ± 1.18 and 10.35 ± 2.33 MPa) and GO (19.49 ± 1.38 MPa and 8.42 ± 2.30 MPa) respectively. Similarly, the ultimate tensile strength values were measured as follows: 6191 ± 2766 kPa for native WH and 1098 ± 615.1 kPa for decellularized WH; 402.7 ± 153.9 kPa for native GO and 73.4 ± 23.6 kPa for decellularized GO; and 872.7 ± 44.5 kPa for native WS and 240.6 ± 100.3 kPa for decellularized WS. The decellularization treatment significantly reduced the maximum elongation of the plants, as shown in Figure 5B. Among the decellularized tissues, WS exhibited the highest elongation, with a maximum value of 7.31 ± 0.64% after decellularization. In comparison, GO and WH showed similar maximum elongations of 2.80 ± 1.13% and 2.37 ± 0.59%, respectively.

Investigations into the suturability of the decellularized plants revealed that WS samples showed the most promise compared to GO and WH samples. As shown in **Figure 6**, the suture retention force in WS (0.184 ± 0.06 N) was significantly higher than in GO (0.059 ± 0.03 N) and WH (0.063 ± 0.02 N). Additionally, suture retention strength (SRS), calculated from the measured forces and taking into account the sample wall thickness, was 2.39 ± 0.84 MPa for WS, 1.42 ± 0.83 MPa for GO, and 1.61 ± 0.69 MPa for WH.

Additionally, the performance of the wet decellularized plants in forming anastomosis was investigated. In general, end-to-end suturing of the decellularized plants to plants and to the animal vessels was feasible as we observed structural integrity at the anastomosis and smooth passage of sutures through the graft wall as depicted in **Figure 7**. During the surgical needle puncturing we detected no crack marks near the puncture sites in the decellularized plants. The loss of tubular shape in some samples of GO increased suture difficulty and time. As anticipated from the suture retention evaluations, we experienced that end-to-end suturing of WS to WS, as well as WS to animal vessels, was significantly easier and more reproducible compared to GO and WH. This was attributed to the higher resistance to rupture during the firm stretch and further knotting.

To enhance our understanding of the potential for further application of decellularized plants, we designed and conducted a multi-stitch tensile strength test. The results of the test on the decellularized plants grafted to porcine arteries demonstrated that WS could withstand greater tensile force compared to the other samples, which was consistent with the findings from the suture retention experiment. By dividing the maximum recorded force by the number of stitches in each sample, the maximum tensile force per stitch was calculated as 0.066 ± 0.003 N for GO, 0.062 ± 0.011 N for WH, and 0.216 ± 0.074 N for WS, which falls within the range of values obtained from the suture retention test.

2.2. Cell Adhesion

Actin filaments and nuclei of the cells are visualized in **Figure 8**. Microscopy revealed that endothelial cells attached and evenly spread on the surface of WS and GO. In contrast, large zones without any attached cells were detected in WH scaffold.

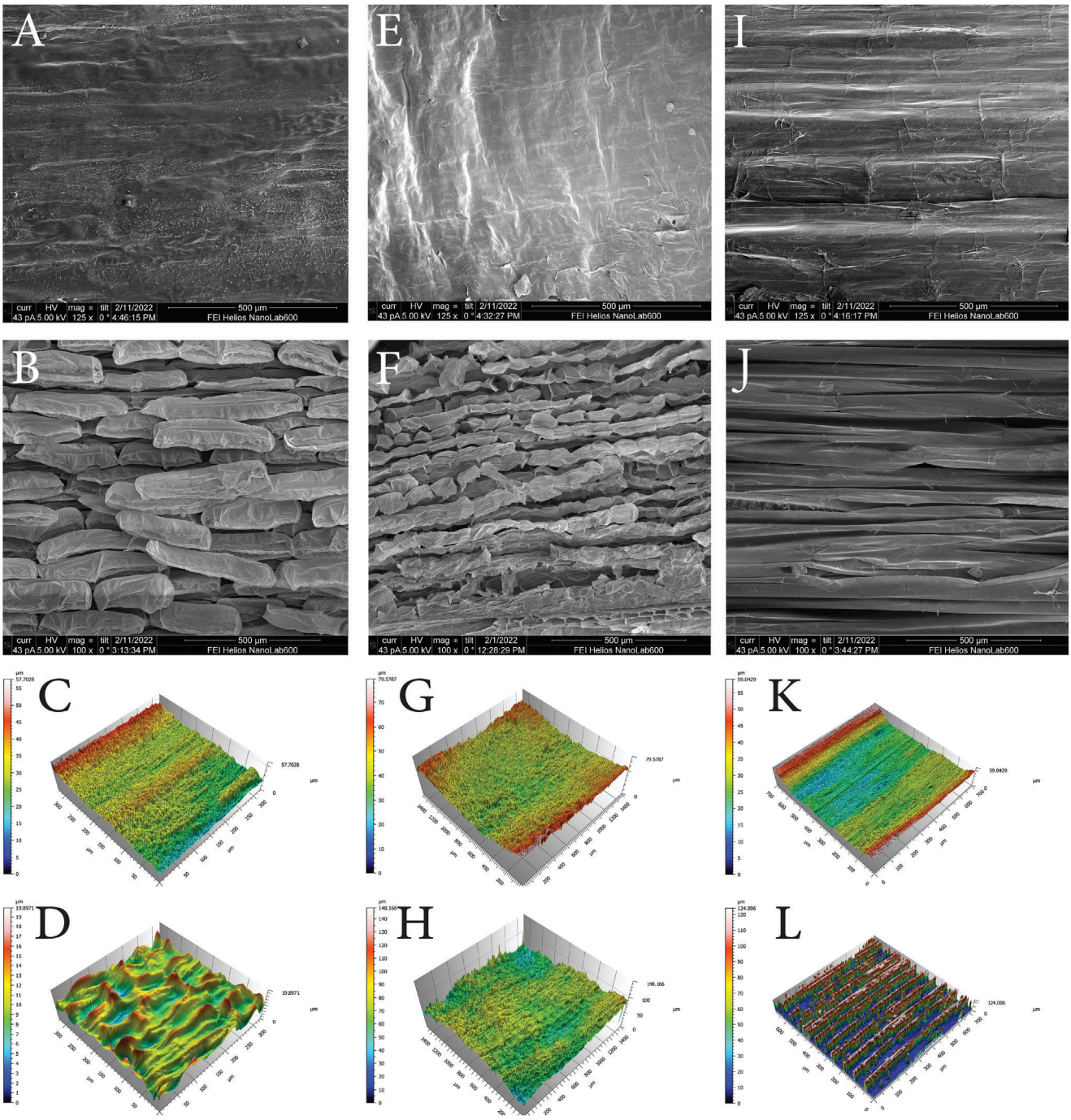

Figure 4. SEM imaging and confocal microscopy of the luminal surface of the plants. SEM images of A) GO before decellularization and B) after decellularization, 3D representations of C) GO before decellularization and D) after decellularization. SEM images of E) WS before decellularization and F) after decellularization, 3D representations of G) WS before decellularization and H) after decellularization. SEM images of I) WH before decellularization and J) after decellularization, 3D representations of K) WH before decellularization and L) after decellularization.

A part of the cells on GO showed elongated morphology (labeled with red arrows), presumably in response to the rectangular cavities on the microstructure while this was not observed on WS. In some regions (labeled with red arrows) on WH, cells were elongated compared to the morphology of cells in TCP, potentially following the parallel groove-like topography of the scaffold.

2.3. Cell Viability

The viability percentage was greater than 80% for TCP, GO, and WS and 70% for WH at every time point (**Figure 9**), suggesting the lack of cytotoxic residues from the decellularization process in the plant structures and indicating no cytotoxic effects from

the chemicals in the selected plants. Additionally, there was no statistically significant difference ($p > 0.05$) observed when comparing the viability of cells cultured on decellularized samples of GO and WS compared to TCP control samples. Nevertheless, the viability rate in WH remained significantly lower than in the other samples on days 2, 3, and 4.

2.4. Cell Proliferation

Immunofluorescence staining of Ki-67 antibody as the proliferation marker of cells on day 1 is illustrated in **Figure 10**A. Quantification of Ki-67-expressing cells on scaffolds and the control group showed significantly more positive cells for this marker on WS and GO in comparison to TCP whereas, no trace of Ki-67 protein was found in the majority of endothelial cells on WH (Figure 10B).

As **Figure 11** presents, on the first day of endothelialization, cell number on the three plant scaffolds was higher than TCP. During the whole period of endothelialization, the number of cells on TCP, GO, and WS steadily increased with a significant rise from day 1 to day 4, while this number decreased in WH. On the last day of endothelialization, significantly fewer cells were observed in WH compared to TCP in contrast to GO and WS, in which more cells were detected.

2.5. Vinculin and VE-Cadherin Expression

Representative images of immunostaining for the Vinculin protein, associated with cell-to-matrix junctions in the focal adhesion complex, on the final day of endothelialization are shown in **Figure 12**A. The average fluorescence intensity of this protein was quantified and is presented in Figure 12B. The cells on all three scaffolds expressed significantly more than 2.5-fold Vinculin in comparison to the TCP control group, with the highest Vinculin intensity nearly equivalent in cells on the GO and WS scaffolds.

Moreover, **Figure 13** shows the VE-cadherin expression in green dye, indicating the endothelial cell-to-cell junctions on the 4th day. In general, HUVECs showing VE-cadherin expression were observed across all three scaffolds as well as in the TCP control group. While in TCP, GO and WS a uniform monolayer of endothelial cells was formed and well-organized cell-to-cell junctions positive for VE-cadherin were visible, this phenomenon was not evident in WH scaffold, where cell clusters were isolated and bounded by cell-free areas.

3. Discussion

The development of biologized tubular scaffolds as vascular grafts and in vitro vessel models is of paramount importance. These scaffolds provide a more physiologically relevant environment, improving vascular regeneration and predictability of preclinical testing for vascular implants and therapeutic interventions. They could consequently reduce reliance on animal models in accordance with the 3R principles (Replacement, Reduction, and Refinement), thereby accelerating the translational success of vascular research.

Considering the great variety of plant kingdom, selection of proper plants and their mechanical characterization after decellularization are fundamental steps toward reliable replication of mammalian tissue properties and consequently use in tissue engineering applications. Decellularized plant tissues primarily consist of cellulose, a biocompatible biomaterial that has been gaining attention in tissue engineering. Promising properties of decellularized plants include biocompatibility,[56,80] non-cytotoxicity,[50,60] cost-effectiveness,[58,59] and owning natural microstructure that facilitates cell adhesion, proliferation, and differentiation.[61,62,64,66] Currently, CelluBridge and CelluJuve products (SPIDERWORT, Ottawa, Canada) from decellularized plants are being used for the regeneration of the spinal cord and the healing of dermal wounds, respectively. However, plant tissues—unlike decellularized animal blood vessels—lack specific polymers and biomacromolecules found in blood vessels that may support endothelialization and tissue remodeling.[46]

Previous research in plant-based vascular tissue engineering has been limited to cultivating endothelial cells either on the planar surface of plant leaves such as Sorghum and Anthurium Magnificum leaves[61,69] or within microchannels of plant leaf petioles and veins including Spinach, Parsley, and Cabbage.[50,58,70,81,82] Gershlak et al. showed that the prevascularized structure of decellularized spinach leaves was similar to the vascular branching structure of a decellularized rat heart. Nevertheless, full endothelialization of leaf microchannels with HUVECs was limited possibly due to the lack of a perfusion-based bioreactor.[50] Walawalkar et al. showed that endothelial cells in the decellularized large leaf scaffold of cabbage proliferate and maintain metabolic activity.[81] Most recently, Cevik et al. introduced a suitable environment of parsley stems for endothelial cell culture and emphasized its potential as a vascular graft. The viability of endothelial cells and collagen deposition by HUVECs on the scaffolds was assessed quantitively and endothelial cells on the scaffolds were qualitatively shown by DAPI and SEM imaging.[58] However, the application of this scaffold is limited due to the narrow inner diameter (<1 mm) of the parsley stem. In our study, we introduced macro-tubular plants with large inner diameters of 3.4 to 6.6 mm to broaden their potential applications. Moreover, to ensure a thorough understanding of the formation of a complete monolayer of endothelial cells on the scaffolds, we considered the importance of visualizing cell junctions and cytoskeleton in addition to staining cell nuclei, which provides a more comprehensive view of cell distribution and scaffold coverage.

To the best of our knowledge, no systematic study on large-diameter tubular plants as potential vascular scaffolds has been carried out. In our study, we investigated three plants with an inner diameter ranging from 3.4 to 6.6 mm, a dimensional range potentially suitable for both vessel-graft implantation as well as biologized in vitro models for research on endovascular implants. We characterized the mechanical and microstructural properties of these tubular plants and assessed their suitability for hosting endothelial cells by investigating their proliferation, cell-to-cell as well as cell-to-scaffold interaction.

Among the variety of tubular plants found in nature, we specifically chose water horsetail, green onion, and water spinach based on logistical aspects (accessibility and availability), dimensional characteristics as well as preliminary experiments, showing their

Table 1. Microstructural characterization of the luminal surface of the plants ($n = 5$).

Sample	Microstructure after decellularization	Sa [µm] native plant	Sa [µm] decellularized	Structure geometry
WH	Parallel grooves	3.41± 0.36	35.80 ± 1.47	Grooves' lateral distance: 64.62 ± 3.11 µm Maximum grooves' peak = 59.42 ± 6.77µm
GO	Rectangular depressions	1.49 ± 0.26	1.78 ± 0.32	Depressions' width: 49.78 ± 4.62 µm Depressions' length: variable
WS	High-density micropeaks	2.15 ± 0.34	3.26 ± 0.23	Longitudinally textured

integrity and stability following decellularization treatment. Significant reduction in the plant DNA and detection of less than 50 ng double-stranded DNA/mg tissue in all three plants confirmed a successful decellularization approach according to common criteria.[83]

In all plants, Young's modulus, ultimate tensile strength (UTS), and maximum elongation decreased after decellularization. Among the parameters, Young´s modulus experienced the highest drop over one order of magnitude or more in all plants. Young´s modulus of the decellularized WS and GO (10.35 ± 2.33 and 8.42 ± 2.30 MPa) was significantly lower compared to WH (73.91 ± 15.69 MPa), yet still higher compared to natural blood vessels which range from 200 kPa to more than 1 MPa depending on the tissue and source.[84–86,87–90] The higher ultimate tensile strength in the WS scaffold compared to GO (240.6 ± 100.3 kPa to 73.4 ± 23.6 kPa) and higher maximum elongation (7.31 ± 0.64% to 2.80 ± 1.13%) might make this plant a more promising scaffold in terms of mechanical similarity to compliant vessels. Nonetheless, previous studies have reported an average of 10% longitudinal strain in the coronary arteries of eight humans and UTS of more than 2 MPa in porcine carotid arteries.[88,91] Moreover, in our study mechanical properties were detected in the longitudinal direction, while the strength in the circumferential direction is more critical during blood pulsation.

The feasibility of suturing plant-to-plant vessels may enable the preparation of modular and longer grafts when more complex anatomies are needed. The anastomosis of plant-derived tubular structures with animal vessels demonstrated the potential feasibility of integrating plant-based grafts with natural tissue. Nevertheless, the suturability of WS was more promising compared to WH and GO. The suture retention of the GO and WH grafts did not align with values reported in the literature; however, the suture retention of WS was within the range of grafts made from natural polymers, as documented in previous studies. In particular, the WS graft in our study showed higher suture retention strength (2.39 ± 0.84 MPa) than the introduced graft from the decellularized parsley stem (0.066 ± 0.029 MPa) by Cevik et al.[58] Moreover, the SRS of 0.184 ± 0.06 N measured in WS is similar to the electrospun Fibrin-PCL grafts introduced by Elliott et al, showing a SRS of 0.21± 0.08 N.[92] Similarly, the SRS for collagen-based grafts amounted to 0.29–0.49 N by Yu et al.[93] Gupta et al. reported 0.38 ± 0.11 N to 0.46 ± 0.11 N suture retention strength for bioresorbable silk grafts,[94] while Wang et al. showed the SRS of 0.45 N for silk fibroin-gelatin vascular grafts.[95] Finally, Cavez et al. reported the SRS of collagen-elastin vascular graft in the range of 0.34–1.88 N.[96] Despite the promising results of WS scaffold, we recognize the potential for improving our grafts' suturability to achieve a higher suture retention force of ≈2N that meets the generally accepted threshold for clinical implantation.[97]

Endothelialization of blood-contacting implants is crucial regarding the inhibition of blood coagulation and platelet activation.[98] Additionally, endothelialized materials potentially replicate the biological environment for conducting in vitro

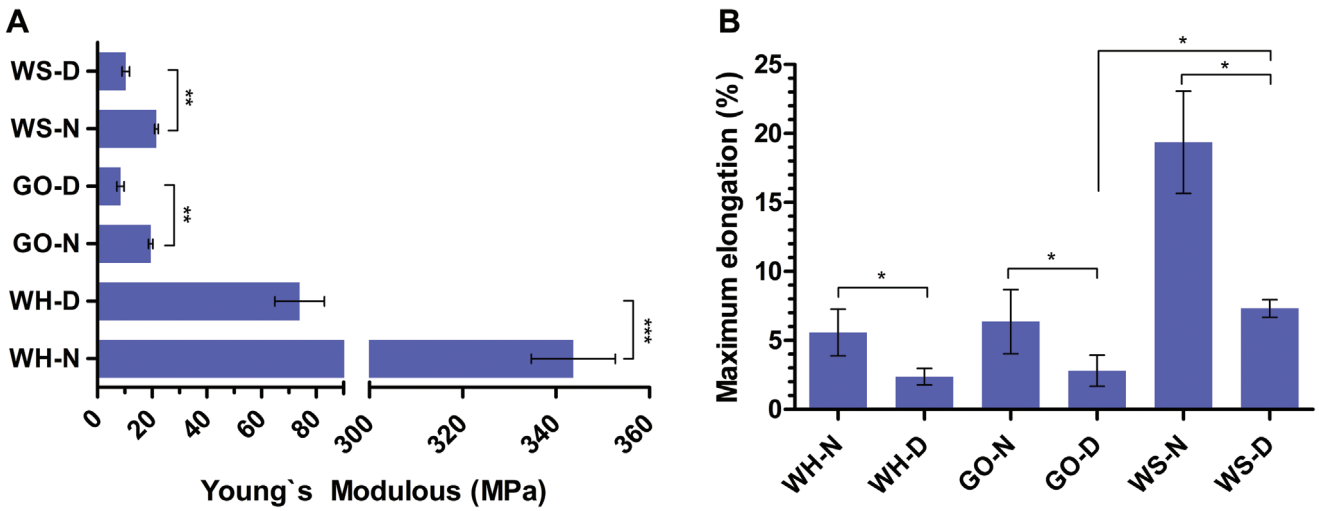

Figure 5. A) Young´s modulus of the decellularized (-D) and native (-N) plants. Figure 5. B) maximum elongation of the plants in decellularized (-D) and native (-N) states ($n = 3$).

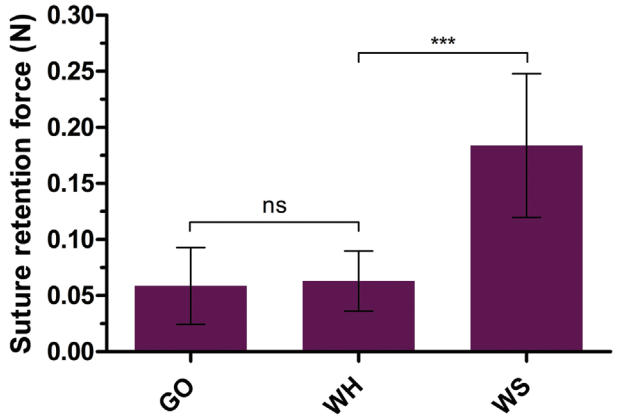

Figure 6. Maximum load depicted as suture retention force (N) measured by tensile machine in decellularized tissues from GO, WH, and WS ($n = 6$).

investigations on cardiovascular implants and pharmaceuticals.[99,33] In this context, the influence of the material surface on endothelial cell proliferation, function, and immunoresponse is crucial.[36] The structure of cellulose can mimic collagen fibers in the natural extracellular matrix (ECM) of animals, forming a 3D matrix that supports tissue regeneration.[100] Since cellulose constitutes the predominant component of post-decellularization plant structures, the resulting substrate can effectively mimic the ECM for cell culture in vitro. In our study, microscopical analysis of the surface properties of the inner sections of the plants performed using scanning electron and confocal microscopy revealed that native plants exhibited smoother surfaces compared to those that had undergone decellularization. The decellularization procedure exposes the underlying microstructure of the plants, perhaps due to the removal of epicuticular wax, which is known to cover plant stems.[101] Consequently, specific surface morphologies were observed on each plant.

As natural vascular tissues have nano-to-microscale features that support the proliferation of endothelial cells,[102–104] it is crucial to notice the correlation between the surface properties of scaffolds and subsequent endothelialization in vitro. The influence of decellularized plant substrates on cell arrangement has been previously reported.[105] Allan et al. showed that nano and micro-grooves on the surface of decellularized amenity grass provide contact guidance supporting myoblast cell alignment and proliferation.[106] Previously, studies by Cheng et al. and Yun et al. showed that groove structures on the outer portion of the white bulb of green onion and Sorghum leaves, respectively, can guide muscle cell alignment.[61,107] In this project, we hypothesized that the natural ECM and microarchitecture of the decellularized tubular plants might stimulate endothelial cells adhesion, proliferation, and interaction with substrate. We observed that actin filaments in endothelial cells are elongated, likely aligning with the microgrooves along the longitudinal axis of WH scaffolds. Additionally, the rectangular surface depressions on the GO scaffolds appeared to impact cytoskeletal rearrangement in some endothelial cells. Among the scaffolds, WS and GO scaffolds enabled homogenous adhesion and distribution of endothelial cells. However, deeper parallel grooves with ≈59 µm elevation might have been responsible for cell-free areas over the surface of WH-scaffolds.

Viability assays during 4 days of endothelialization did not reveal any cytotoxic effect of the prepared scaffolds on endothelial cells. Ki-67, a protein that is expressed in the nuclei of proliferating cells, is a well-known marker for assessing cell proliferation.[108,109] Physical, chemical, and mechanical properties of substrates can affect proliferation of endothelial cells and further expression of Ki-67.[110,111] Investigating the number of ki-67 positive endothelial cells has been used for the comparison of their proliferation capability in vitro and in vivo as well as in therapeutic applications where angiogenesis evaluation was required.[112–115] Higher expression of the Ki-67 gene in the GO and WS scaffolds than in WH could be correlated to the more suitable microenvironment of those scaffolds for endothelial cell proliferation while presumably, the unsuitable surface topography of the WH scaffold appears to suppress the proliferation of HUVECs. Significantly higher visualization of Ki-67 positive HUVECs in GO and WS scaffolds compared to TCP could be correlated to the surface microstructure of these scaffolds as well as collagen coating similar to previous studies that showed elevation of proliferation and Ki-67 expression in the presence of collagen type I.[116,117]

A higher number of adhering cells on all the plant scaffolds compared to TCP was detected on the first day of endothelialization. The number of cells on WH decreased until day 3 of the experiment and did not change significantly from day 3 to day 4. This matter is consistent with the lowest expression of Ki-67 protein on this scaffold. We observed a constant increase in the number of detected cells on WS and GO during 4 days of endothelialization. Significantly more adhesion of cells on all the plant scaffolds compared to TCP at day 1 might be due to the surface modification of scaffolds via collagen coating, available 3D topography as well as higher specific surface area of the decellularized plants. Since surface roughness is a well-known factor influencing HUVEC proliferation,[118,119] we were eager to explore the effect of the scaffold's surface roughness on endothelialization. Higher cell proliferation in GO and WS with surface roughness of $Sa = 1.78 \pm 0.32$ and 3.26 ± 0.23 µm, respectively is aligned in some way with previous findings indicating enhanced cell proliferation on surface roughness of 2 µm compared to a smooth surface.[120] However, sub-micron roughness on other biomaterials was introduced as the best surface topography for endothelial cell attachment and proliferation.[44,121,122] Nevertheless, considering that more factors such as cell type, material surface chemistry, and mechanical properties, particularly stiffness and elasticity play an important role in cell behavior,[123,124] direct comparisons of the influence of roughness between our results and those of earlier studies with different study parameters could not be done.

Since instability of cells in endothelialized scaffolds has been a limitation in previous studies, it is crucial to evaluate and improve the adhesion strength of endothelial cells on scaffolds and finally prepare tissue-engineered vessel models with more stable endothelium.[37,38,40,125] Interactions of Vinculin as a key protein in focal adhesion complexes (FAC) and cell integrins mediate the anchorage of endothelial cells to the surrounding ECM.[126] Investigating Vinculin expression provides insights into cell adhesion strength.[127] Higher secretion of Vinculin from HUVECs

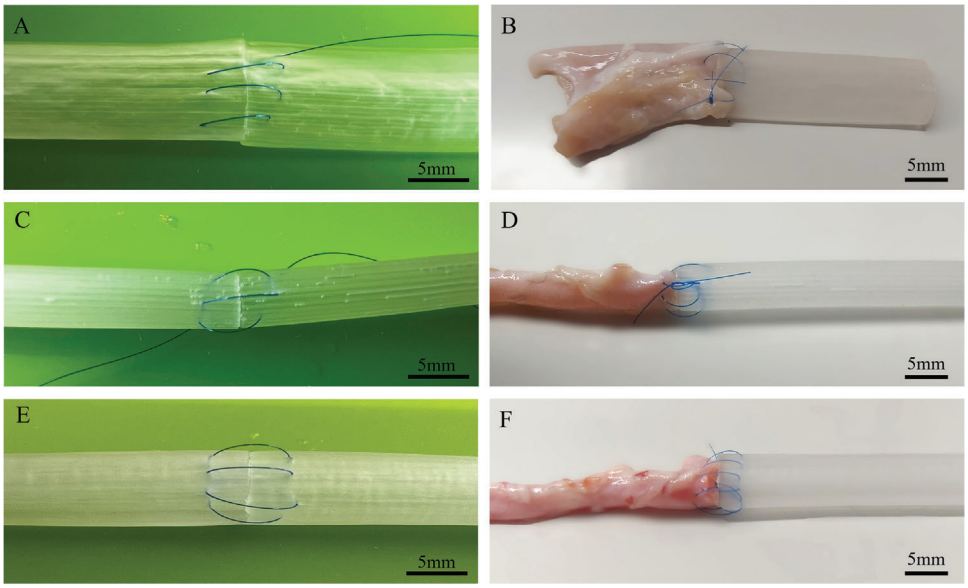

Figure 7. Representative images of end-to-end suturing of decellularized GO, WH, and WS plants. A) GO to GO and B) GO to freshly dissected porcine pulmonary artery. C) WH to WH and D) WH to freshly dissected porcine coronary artery. E) WS to WS and F) WS to freshly dissected porcine coronary arteries.

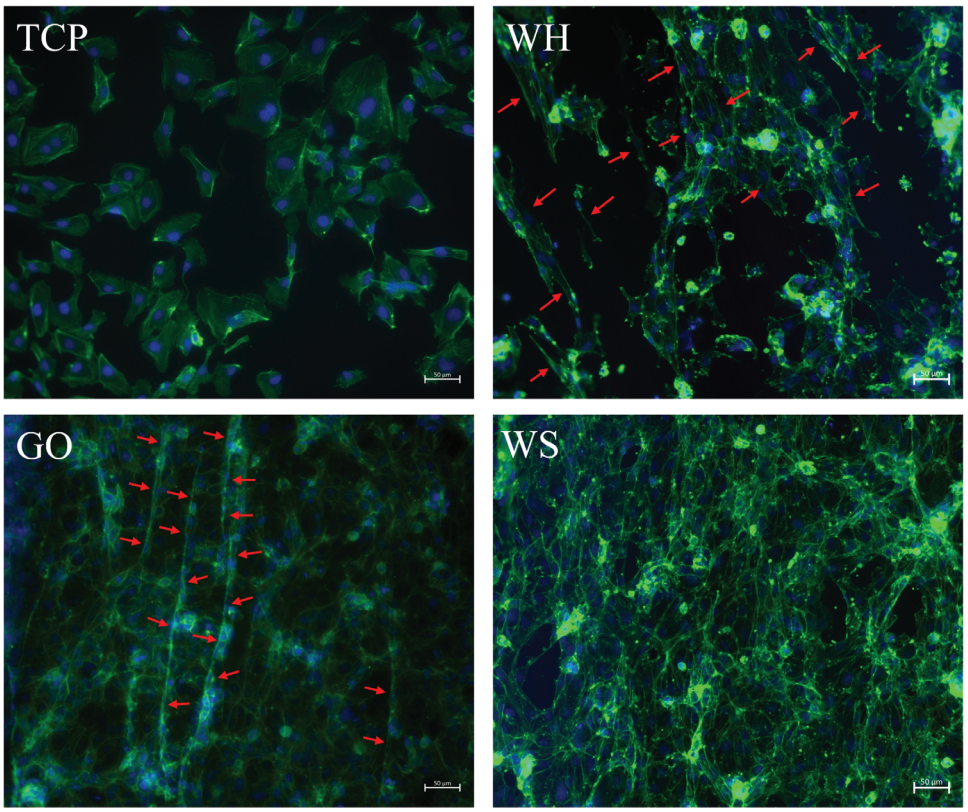

Figure 8. Actin filaments (green) and nuclei (blue) staining of the HUVECs on tissue culture plate (TCP) surface, WH, GO, and WS scaffolds.

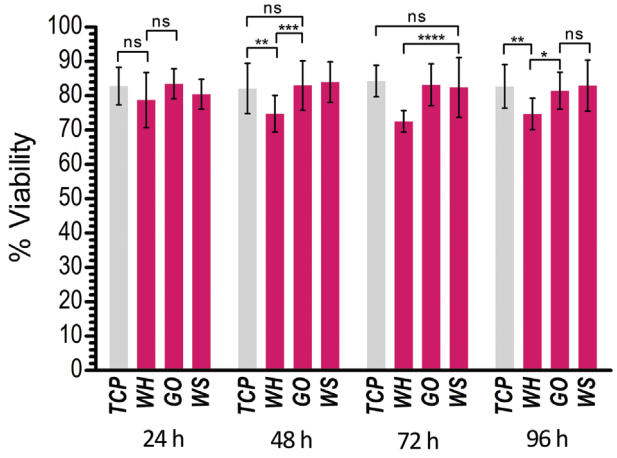

Figure 9. Viability of HUVECs on TCP, WH, GO, and WS after 24, 48, 72, and 96 h ($n = 3$).

on WH, GO, and WS scaffolds to those cultivated on the 2D environment of TCP declared stronger adhesion of endothelial cells on the prepared 3D scaffolds. Previously, the quantification of the Vinculin fluorescence signal was reported to be 3-fold higher in endothelial cells on 3D gelatin scaffold in comparison to 2D substrates.[128] Our results show that the topological features on the surface of the prepared decellularized plant scaffolds increased endothelial cells' focal adhesion. It seems that the cells adhering to the WH scaffold on day 4, though fewer in number compared to other scaffolds, had a robust attachment to the provided 3D environment. This phenomenon arises from the fact that Vinculin measurement in this study was derived from the average Vinculin signal detected from adhered cells, rather than being based on the total number of cells on scaffolds. Nevertheless, more Vinculin expression from endothelial cells on GO and WS, compared to all other groups, can suggest stronger cell adhesion to the substrates, consequently making them more promising substrates for the fabrication of endothelialized scaffolds.

VE-cadherin, a distinctive marker of endothelial cells, functions as a central transmembrane protein localized at the interface of neighboring cells, facilitating tight junction formation and cell-to-cell interaction within an endothelialized substrate.[129] In this light, we explored the formation of endothelium on the prepared scaffolds by this marker. The low expression of this marker in WH accounts for the incomplete endothelialization on the scaffold surface. In contrast, the establishment of a confluent monolayer of endothelial cells on GO and WS confirmed by VE-cadherin staining revealed the confluent endothelialization by the end of the experiment.

While our study aimed to characterize some decellularized tubular plants and investigate their endothelialization, several limitations should be considered. Given that the tubular scaffolds introduced in this study are derived from natural plant sources, the geometry of the samples cannot be readily manipulated or controlled. We observed variations in wall thickness and deviations from a perfectly circular cross-section in these plant-based scaffolds, which may affect their mechanical properties and present challenges during anastomosis. However, due to their high availability and low cost, we recommend pre-selecting samples with more uniform wall thickness and cross-sectional geometry to enhance their applicability as grafts. Plant species may display diverse growth patterns across various zones and environments, potentially influencing their dimensions and mechanical properties. Consequently, this variability could impact the reproducibility of plant growth for the fabrication of tubular scaffolds. The higher mechanical properties of the introduced tubular scaffolds compared to native tissues still represent a limitation concerning their further applications. Therefore, further studies to adjust and improve the mechanical properties of decellularized plants are needed.

Endothelialization was performed on planar scaffolds derived from the plant's tubular structures to achieve a more reproducible and geometry-independent investigation of the microenvironment effect on endothelial cells. This approach excludes the cross-effects of the plant's inner diameter and facilitates microscopic assessment. However, effective endothelialization of the entire luminal surface of the tubular plants – such as by means of a bioreactor – has to be verified in future investigations as a prerequisite for realization of biologized vessel models and vascular grafts. Investigating endothelialization of the introduced scaffolds during a longer period as well as using more robust assays for evaluation of cell proliferation such as XTT could be performed in the future. Moreover, in our study, all the plant scaffolds were coated with collagen using the same procedure, whereas TCP, serving as the control group, was not coated. Therefore, a comparison between both plant scaffolds and TCP with collagen coating might provide a fairer assessment of the influence of surface topography on endothelialization and could be considered for future research.

As endothelial cell alignment and spatial orientation are highly correlated with tissue functionality in vivo and in vitro,[130] further assessment of the secretion of immunomodulatory factors from endothelial cells on the scaffolds and comparison to the control environment could be carried out. Upon reviewing the outcomes of our study, we see possibilities for additional investigation within this field. Since endothelial cells respond to the environmental shear stress by cytoskeletal re-arrangement, alteration in gene expression, nitric oxide production and functionality,[131] investigations of endothelial cell behavior under physiological flow conditions appear to be a reasonable advance. Looking ahead, we plan a first feasibility study of stent implantation within a decellularized and endothelialized tubular plant. In preliminary experiments, we tested the integrity of the presented scaffolds after catheter-based deployment of a self-expandable stent with a diameter of 6 mm and length of ≈15 mm, manufactured in-house using a 100 µm nitinol wire. (Figure S1 and Video S1, Supporting Information).

We acknowledge the extended possibilities presented by the endothelialized scaffolds as a novel vessel model for preclinical implant investigations in cardiovascular research as well as potential cost-effective and sustainable plant-derived vascular grafts.

4. Conclusion

In this study, we analyzed the macroscopic and microscopic properties of three tubular plant specimens before and after decellularization, to prepare endothelialized scaffolds. Water

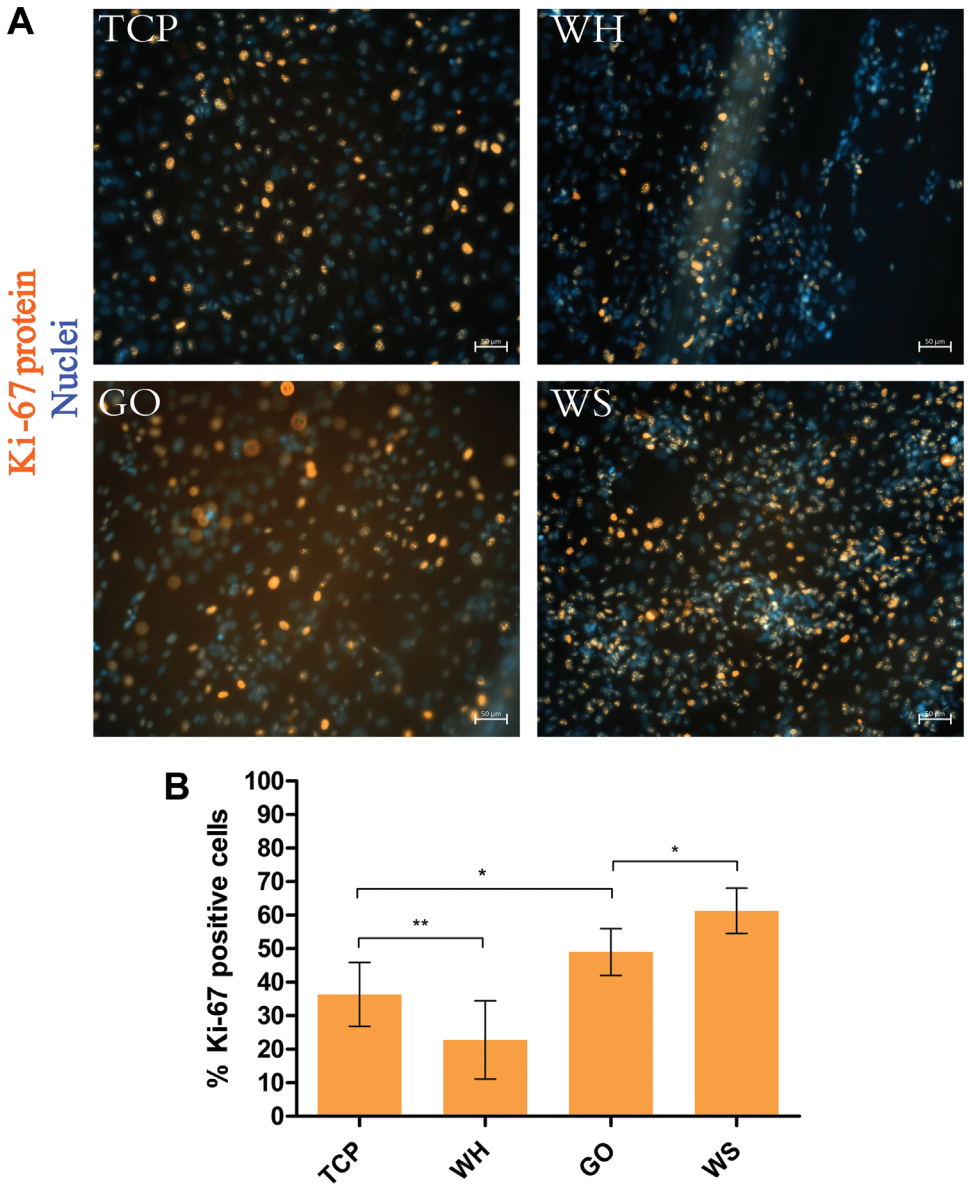

Figure 10. A) Immunofluorescence staining of Ki-67 protein (orange) and DAPI staining of HUVECs nuclei (blue) on TCP, WH, GO, and WS. B) Percentage of HUVECs expressing Ki-67 protein on TCP, WH, GO, and WS ($n = 3$).

horsetail, green onion, and water spinach plant which kept their consistency after decellularization, were selected for further assessments. Each plant showed unique microstructure and mechanical properties. Regarding their potential use as a graft, we found the suturability of decellularized water spinach to be the most favorable. While the mechanical properties of the introduced plants do not match those of animal tissues, decellularized water spinach exhibits the most promising mechanical characteristics among the other scaffolds. Excessively high Young´s modulus, and low ultimate elongation besides the hindered proliferation and formation of a monolayer of endothelial cells in water horsetail render this scaffold less promising. However, during endothelialization of water spinach and green onion, the number of cells increased constantly, and Ki-67 proliferative protein was significantly higher expressed in these scaffolds compared to the control group. Perhaps, in contrast to water horsetail, the microenvironment of green onion and water spinach scaffolds eased the endothelialization process. Upon conducting VE-cadherin immunostaining of cells at the final time point, we observed the development of endothelium on the surfaces of green onion and water spinach scaffolds. Immunofluorescent staining of vinculin on the endothelialized scaffolds further demonstrated the possibility of strong cell attachment to the water spinach and green onion substrates compared to other materials. In the end, endothelialized tubular scaffolds from green onion and water spinach might represent future biomaterials for different applications in vascular tissue engineering, including in vitro research models. Considering the suturability of decellularized

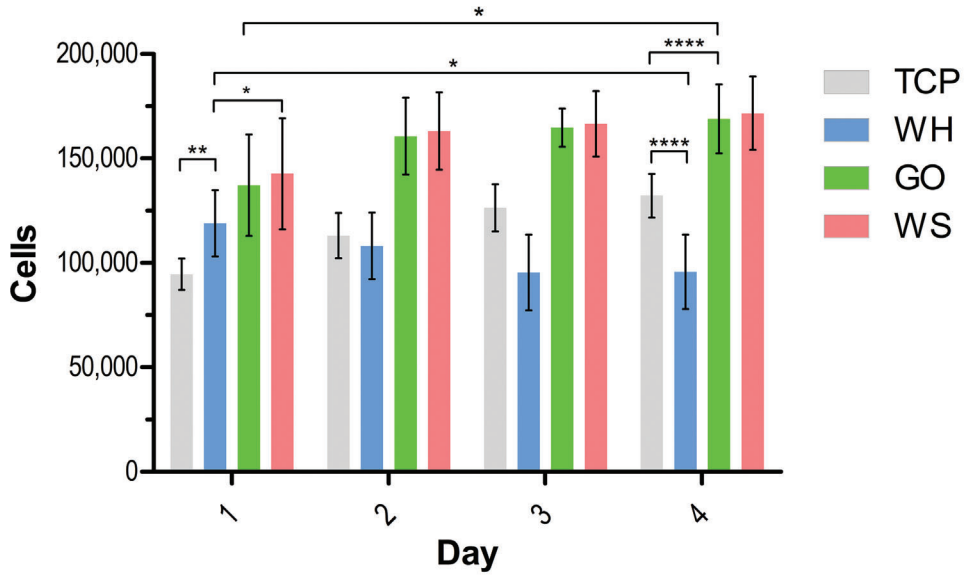

Figure 11. The number of counted HUVECs on the control group of TCP, WH, GO, and WS scaffolds on days 1, 2, 3, and 4 ($n = 3$).

water spinach, this tubular scaffold shows the highest potential for use as a vascular graft.

5. Experimental Section

Plant Decellularization and Dimensional Characterization: A preliminary selection of plants (Table S1, Supporting Information) was carried out based on the criteria of tubularity in structure or stem, stability of hollow tissue, flexibility, and desired dimension. Water Spinach (Ipomoea aquatica), Water Horsetail (Equisetum hyemale japonicum), and Green Onion (Allium fistulosum) were selected and purchased from the local market to obtain sufficient native and decellularized tissues for the following experiments, each performed in triplicate ($n = 3$). Tubular structures derived from stems of Water Horsetail (WH), Water Spinach (WS), and Green Onion (GO) were decellularized according to the organ perfusion decellularization technique. In short, the plant tissues were immersed consecutively in pure solutions of Hexane (purity ≥ 94.5%, Sigma-Aldrich, Germany) and phosphate-buffered saline (PBS) (Sigma-Aldrich, Germany) three times each for 5 minutes, to remove waxy cuticles from the plant tissues and therefore to allow the chemicals used for decellularization to permeate the tissue more efficiently. Then, the stems were immersed in a 10% sodium dodecyl sulfate (SDS) (Bioreagent, ≥ 98.5%, Sigma–Aldrich, Germany) solution in deionized water for 5 days with gentle agitation of the samples on a shaker (rpm = 70, T = 25 °C). Consequently, they were washed 3 times with deionized water followed by rinsing in a 0.1% Triton X-100 (Sigma–Aldrich, Germany) and 10% sodium hypochlorite solution (EMPLURA, Merck, Germany) for 2 more days under the same mentioned conditions. At day 7, the samples were washed thoroughly in a deionized water bath for 3 min and the step was repeated three times with fresh water to remove the chemical residues from the plants. Once the protocol was finished, they were stored in deionized water in the refrigerator, at a temperature of ≈4 °C, for further use. Finally, the dimensions of the decellularized tubular plants ($n = 6$) were characterized by cutting samples and taking cross-sectional images using a Stereomicroscope (Leica S9D, Germany).

DNA Quantification: Native and decellularized samples were immersed in liquid nitrogen and pulverized with a mortar and pestle. Consequently, 50 mg of plant tissues were added to 2 mL Eppendorf tubes containing 400 µL of pre-warmed (65 °C) extraction buffer with a PH of 6.8 containing 100 mM Tris-HCl, 700 mM NaCl, and 50 mM EDTA. After cooling the samples, 220 µL of chloroform/ isoamyl alcohol (24:1) was added and the sample was shaken gently for 5 min followed by 2 min centrifuge at 70 000 rpm. The supernatant was mixed with 400 µL isopropanol, allowed to precipitate for 2 min at RT and then centrifuged for 10 min at 70 000 rpm. The supernatant was removed, and the pellet was washed with 350 µL 70% ethanol, followed by centrifuging for 2 min at 70 000 rpm. The supernatant was carefully removed and the pellet was allowed to dry for 10 min at RT and 30 µL of dd-H2O was added and the DNA was dissolved at 65 °C for 10 min. The extracted DNA was quantified using a spectrometer (BioTek Epoch2, USA).

Scanning Electron Microscopy: Native and decellularized tissues from the selected plant were placed in −20 °C freezer for 2 h and then immersed in liquid nitrogen for 1 min and subsequently lyophilized (Heto Power Dry LL3000 Freeze Dryer). The freeze-dried samples were coated via a spinning gold sputtering device and the inner surface of tubular plants was imaged with FEI Helios NanoLab600 scanning electron microscope at a voltage of 5 kV.

Confocal Microscopy: The walls of tubular plants in both decellularized and native states were sectioned to create samples measuring 10 × 10 mm. These samples were thoroughly washed three times with deionized water (Sigma–Aldrich, Germany) prior to microscopy. The samples were fixed onto the specimen stage, and the luminal surfaces of the plants were imaged using contact-free confocal microscopy (MarSurf CM Expert, NanoFocus AG, Germany) in CSI mode with a magnification of 10x (NA 0.3, FOV 1.6 × 1.6 mm^2) to facilitate a comprehensive and representative analysis of surface topography across larger areas. To correct for any tilt or curvature in the samples, Least-Squares Plane Leveling (LSPL) was applied to the acquired data, ensuring an accurate baseline for surface roughness and topography analysis. The images were processed in accordance with ISO 25178-2 via the associated MarSurf MfM (Extended 8.2.9564, NanoFocus AG, Germany) software and the arithmetical mean height of the surface (Sa), grooves' lateral distance and maximum grooves' peak (in WH) and depressions' width (in GO) were measured in 5 repeats on five distinct zones within the lumen of one representative standard sample from each plant.

Mechanical Characterization: For the mechanical characterization of native and decellularized plants, tensile test was performed using a tensile testing machine (INSTRON 34SC-1, USA) with a 50 N force capacity. Measurements for 3 samples of each plant species in both their native and decellularized state were obtained. To perform the test, 120 mm long samples were cut and the tensile velocity of 5 mm min^{-1} was applied. Young's

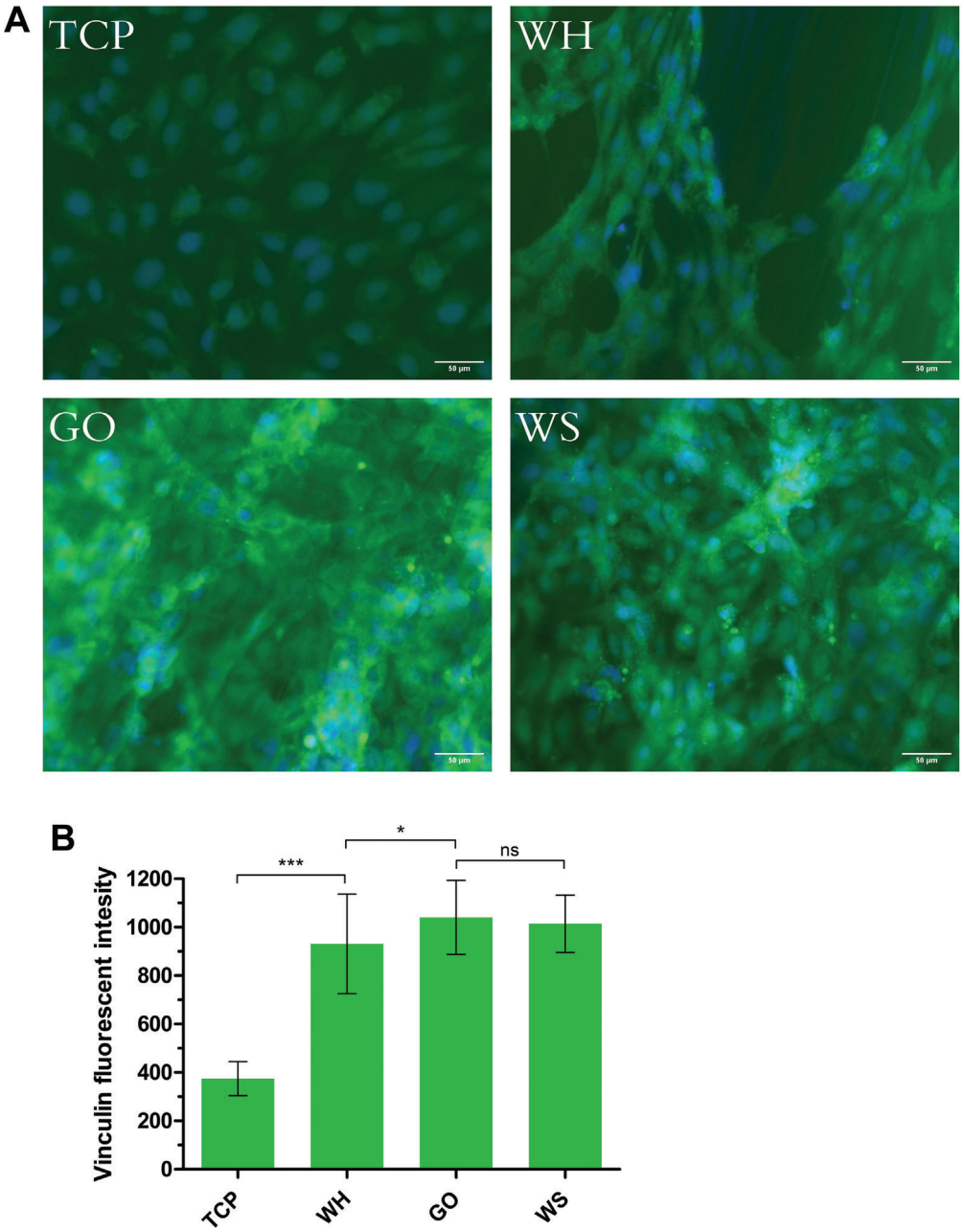

Figure 12. A) Representative images of Vinculin immunostaining (green) and DAPI (blue) of HUVECs on the substrates at the last day of endothelialization. B) Intensity of Vinculin expression from the HUVECs cultivated on WH, GO, WS, and the control substrate of TCP ($n = 3$).

modulus as the slope of the linear section of the stress–strain graph in a strain range between 0.01% and 0.5%, elongation at maximum stress and ultimate tensile strength (UTS) were derived from the stress–strain curve.

Suture retention strength of the tubular scaffolds was determined according to the American National Standard Institute–Association for the Advancement of Medical Instruments (ANSI/AAMI) VP20 standards.[132] The wet decellularized plants were cut open longitudinally to obtain rectangular strips ($n = 6$, length = 40 mm) with the short edge of each specimen belonging to the circumference of the tubular scaffolds. A single 6-0 polypropylene (ATRAMAT, Mednaht, Germany) suture was used to create a single loop 2 mm away from the short edge of the scaffolds and at equal distance from both long edges. The free end of the suture was fastened with laboratory labeling tape (Sigma–Aldrich, Germany), positioning the scaffolds at the center of the loop. The tape was then clamped in the upper grip of the tensile testing machine. The other end of the scaffold strip was secured in the lower grip, and the suture was pulled at a constant rate of 5 mm min^{-1} along the scaffold's longitudinal axis until it ruptured. The maximum load measured was recorded as the suture retention force and the suture retention strength (SRS) was calculated as suture retention force/(suture diameter × sample wall thickness).

The suturing feasibility and preparation of modular grafts from decellularized plants was first evaluated by suturing two decellularized plants of each type ($n = 3$) with a surgical needle (3/8 circle premium round needle, ATRAMAT, Mednaht, Germany) and the 6-0 polypropylene suture,

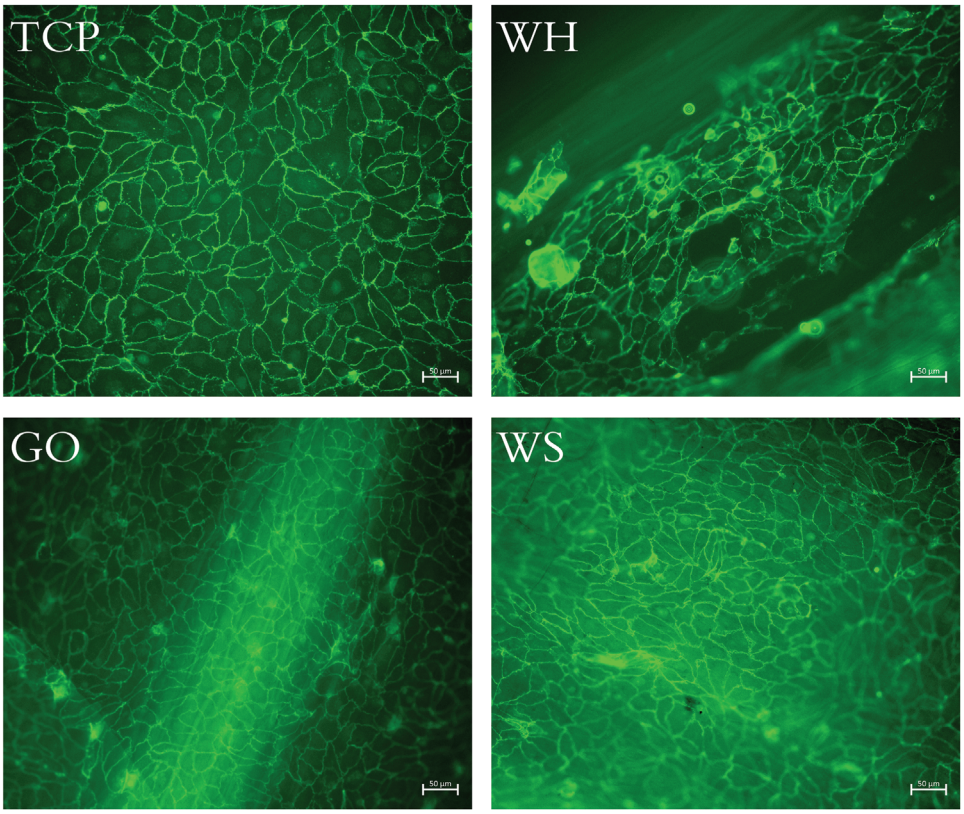

Figure 13. Immunofluorescence staining of VE-cadherin in HUVECs on TCP, WH, GO, and WS.

described above. Furthermore, to gain further insights into the potential applications of the decellularized plants in anastomosis, three replicates of each decellularized plant type were end-to-end sutured ≈2 mm away from the sample edge onto freshly dissected porcine coronary arteries (for WH and WS scaffolds) and pulmonary artery (for GO scaffold) obtained from three different animals. Finally, the grafted plants to coronary and pulmonary arteries underwent a multi-stitching strength test by clamping both ends of the wet grafts to the grips of the tensile machine and pulling uniaxially at a rate of 1mm min^{-1} until the sutures broke completely free from the scaffold wall ($n = 3$). The burst force was divided by the number of stitches to obtain the maximum tensile force per stitch.

Scaffold Preparation: To generate a hydrophobic surface inhibiting cell adherence, polydimethylsiloxane (PDMS) coating was applied at the bottom of each well of 24-well tissue culture plates. For that, a 1:10 solution of the elastomer curing agent to elastomer base (Sylgard 184, DOW, USA) was transferred to each well and cured at 85 °C for 2 h. The plates were allowed to cool to room temperature and washed thoroughly with PBS to remove unreacted reagents. The decellularized tissues of GO, WH, and WS were punched to fit the size of a well of a 48-well plate. After that, the scaffolds were sterilized using 70% Ethanol and UV irritation following washing in PBS. Subsequently, the scaffolds were placed on PDMS-coated wells. The surface of decellularized plants was modified with collagen coating according to the reported established method.[57,74] Briefly, the scaffolds were incubated for 4 h at room temperature in a solution of 5 µg mL^{-1} collagen (Type I, rat tail, Ibidi) in acetic acid followed by washing in PBS before use. The scaffolds were carefully positioned within the wells, ensuring that the luminal surface of the tissues faced upward to come in contact with seeding cells.

Cell Culture: Human Umbilical Vein Endothelial cells (HUVEC) isolated in growth medium 2, pooled, (PromoCell, Germany) were cultivated with Endothelial Cell Growth Medium 2 Kit (Promocell, Germany) until 80% confluence. Cell suspension of 470 × 10^3 cells mL^{-1} was prepared from HUVECs passage number 3 and 450 µL of the suspension was seeded on top of each scaffold and wells of tissue culture plate (TCP) with Nunclon Delta treatment as a control group. The scaffolds and control group were incubated in a cell culture incubator at 37 °C, 5% CO_2 overnight before the first medium change, and after that, the medium was changed every two days for the rest of the experiment.

Cell Adhesion, Proliferation, and Viability Assays: F-Actin staining solution (CytoPainter, green fluorescence, Abcam, Germany) was used to observe the actin filaments within the cytoskeleton of the fixed cells on day 1 and thus assess cell adhesion and distribution over the scaffolds´surface and possible change in the arrangement of cells cytoskeleton. Immunofluorescent staining of samples by assessing expression of Ki-67 protein in the nuclei of 4′, 6-diamidino-2-phenylindole (DAPI) stained cells to investigate endothelial cells proliferation potency was performed on day 1. Cells on each sample were washed thrice with PBS and then fixed with 1% Paraformaldehyde (PFA) solution for 10 min. After being permeabilized with 0.01% Triton X-100 for 3 min, the cells were blocked by 10% normal goat serum for 30 min. After overnight incubation of samples with Ki-67 antibody staining solution (Alexa Fluor 555 conjugated, Cell signaling technology, USA) in 1.5% normal goat serum at 4 ° C and further washing, 10 random zones on each sample were imaged and the number of total cells and Ki-67 positive cells were calculated.

Endothelial cell proliferation on the prepared scaffolds and control samples was investigated by DAPI staining on days 1,2,3, and 4. Prior to the staining, the cells were fixed with 4% PFA (Alfa Aesar, USA) in PBS for 20 min and subsequently washed 3 times with PBS. Afterward, the cells that had been fixed on scaffolds and TCP were subjected to DAPI staining solution (Abcam, Germany) to visualize the nuclei of the cells. The proliferating cells were quantified by counting the nuclei in 10 randomly chosen images per sample, which covered the majority of the surface area.

On 1, 2, 3, and 4 of endothelialization, the cells on scaffolds and control samples were washed with PBS after 15 min of incubation of samples in a

cell culture incubator and the viability of the cells was determined based on two-color fluorescence analysis of Propidium Iodide and Hoechst, using LIVE/DEAD Cytotoxicity Assay Kit (Abcam, Germany). The number of live and dead cell from 20 random regions of each sample were counted. All the fluorescent images were obtained using a ZEISS Axio Vert.A1 inverted fluorescent microscope (Carl Zeiss Suzhou Co., Ltd.) and provided software of ZEISS ZEN 3.7. Quantification of cells was facilitated by BioApps software, Zen Blue, Zeiss.

Immunofluorescence Analysis of Cell-to-Cell and Cell-to-Substrate Junctions: Similar to the previously described method, the cells were fixed, permeabilized, and blocked before immunofluorescent staining. On the final day of the endothelialization, VE-cadherin antibody (Alexa Fluor 647 conjugated, Santa Cruz Biotechnology, Inc., USA) was employed as the specific marker for endothelial cells, staining the intracellular junctions of HUVECs. Representative images of each sample were captured via fluorescence microscopy.

Additionally, the adhesion of endothelial cells to the substrates was evaluated via Vinculin antibody staining (Recombinant Alexa Fluor 488 Anti-Vinculin antibody, Abcam, Germany) on day 4 and further DAPI staining to locate cells' position. The assessment of Vinculin within the cell was conducted through fluorescence intensity analysis. Specific areas of single cells were chosen, and the levels of green channel intensity were measured using Zeiss image analysis software. This procedure was repeated for every cell culture condition and the arithmetical mean intensity of reflected VE-cadherin signals from 25 single cells of each sample were measured.

Statistical Analysis: All experiments in this study were performed with three repeats ($n = 3$) unless otherwise specified, and the results are presented as the mean value ± standard deviation (SD). The data from each group were compared using two-way ANOVA analysis for Figures 3 and 5A,B and 9 and 11 and one-way ANOVA analysis for Figures 6 and 10B and 12B conducted with Graph Pad Prism software, with significant differences between various groups reported when the P-values were below 0.05. The symbols *, **, ***, and **** represent significance levels of $p < 0.05$, 0.01, 0.001, and 0.0001, respectively.

Supporting Information

Supporting Information is available from the Wiley Online Library or from the author.

Acknowledgements

The Authors would like to thank: the Ministry of Science, Research and the Arts Baden-Württemberg and the University of Stuttgart for funding this project (RISC), which enabled us the successful completion of this study. Prof. Dr. Monilola Olayioye and Prof. Dr. Angelika Hausser, Institute of Cell Biology and Immunology. Prof. Dr. Arnd G. Heyer, Institute of Biomaterials and Biomolecular Systems, University of Stuttgart for providing us with the infrastructure to perform DNA quantification assay. The Institute of Applied Optics for providing us with the SEM equipment and M.Sc. Holger Ruehl for support in SEM imaging. Dr. Mario Hentschel and 4th Physics Institute and Research Centre SCoPE of the University of Stuttgart for providing us with the infrastructure for confocal microscopy. All the team members of the Institute of Biomedical Engineering, University of Stuttgart.

Open access funding enabled and organized by Projekt DEAL.

Conflict of Interest

The authors declare no conflict of interest.

Data Availability Statement

The data that support the findings of this study are available from the corresponding author upon reasonable request.

Keywords

biomimetic, decellularized plants, endothelialization, HUVECs, tubular scaffolds, vascular tissue engineering

Received: July 15, 2024
Revised: November 8, 2024
Published online: December 4, 2024

[1] M. E. DE Bakey, D. A. Cooley, E. Stanley Crawford, *AMA Arch Surg.* **1958**, *77*, 713.
[2] J. M. Johnson, D. Goldfarb, L. D. Baker, *Am. J. Surg.* **1976**, *132*, 723.
[3] P. Field, *Cardiovasc. Surg.* **2003**, *11*, 30.
[4] M. Bossi, M. Tozzi, M. Franchin, S. Ferraro, N. Rivolta, M. Ferrario, C. Guttadauro, P. Castelli, G. Piffaretti, *Ann Vasc Dis* **2017**, *10*, 391.
[5] H. DARDIK, DARDIK II, *Ann. Surg.* **1976**, *183*, 252.
[6] F. Jafarihaghighi, M. Ardjmand, A. Mirzadeh, M. S. Hassani, S. S. Parizi, *Cell Tissue Bank* **2020**, *21*, 377.
[7] D. F. LaRosa, A. H. Rahman, L. A. Turka, *J. Immunol.* **2007**, *178*, 7503.
[8] J. A. Fishman, L. Scobie, Y. Takeuchi, *Xenotransplantation* **2012**, *19*, 72.
[9] S. Huerta, A. Varshney, P. M. Patel, H. G. Mayo, E. H. Livingston, *JAMA Surg.* **2016**, *151*, 374.
[10] I. Ribitsch, P. M. Baptista, A. Lange-Consiglio, L. Melotti, M. Patruno, F. Jenner, E. Schnabl-Feichter, L. C. Dutton, D. J. Connolly, F. G. van Steenbeek, J. Dudhia, L. C. Penning, *Front. Bioeng. Biotechnol.* **2020**, *8*, 972.
[11] J. J. Hu, W. C. Chao, P. Y. Lee, C. H. Huang, *J. Mech. Behav. Biomed. Mater.* **2012**, *13*, 140.
[12] L. Soffer, X. Wang, X. Zhang, J. Kluge, L. Dorfmann, D. L. Kaplan, G. Leisk, *J. Biomater. Sci. Polym. Ed.* **2008**, *19*, 653.
[13] N. C. Paxton, R. Daley, D. P. Forrestal, M. C. Allenby, M. A. Woodruff, *Mater. Des.* **2020**, *193*, 108787.
[14] A. M. van Genderen, K. Jansen, M. Kristen, J. van Duijn, Y. Li, C. C. L. Schuurmans, J. Malda, T. Vermonden, J. Jansen, R. Masereeuw, M. Castilho, *Front. Bioeng. Biotechnol.* **2021**, *8*, 617364.
[15] M. J. J. van Velthoven, R. Ramadan, F. S. Zügel, B. J. Klotz, D. Gawlitta, P. F. Costa, J. Malda, M. D. Castilho, L. M. O. de Kort, P. de Graaf, *Tissue Eng. Part C Methods* **2020**, *26*, 190.
[16] Y. Jung, H. Ji, Z. Chen, H. Fai Chan, L. Atchison, B. Klitzman, G. Truskey, K. W. Leong, *Sci. Rep.* **2015**, *5*, 15116.
[17] M. Rabionet, A. J. Guerra, T. Puig, J. Ciurana, *Vasc. Tissue Eng. Proc. CIRP* **2018**, *68*, 352.
[18] A. J. Boys, S. L. Barron, D. Tilev, R. M. Owens, *Front. Bioeng. Biotechnol.* **2020**, *8*, 589960.
[19] B. H. Walpoth, H. Bergmeister, G. L. Bowlin, D. Kong, J. I. Rotmans, P. Zilla, *Tissue-Engineered Vascular Grafts*, Springer International Publishing, Berlin/New York **2020**.
[20] S. Pashneh-Tala, S. MacNeil, F. Claeyssens, *Tissue Eng. Part B Rev.* **2016**, *22*, 68.
[21] J. Fernández-Pérez, K. A. van Kampen, C. Mota, M. Baker, M. L. Flexible, *ACS Biomater. Sci. Eng.* **2023**, *9*, 5006.
[22] X. Meng, X. Wang, Y. Jiang, B. Zhang, K. Li, Q. Li, *RSC Adv.* **2019**, *9*, 21258.
[23] X. Chen, Y. Yao, S. Liu, Q. Hu, *J. Biomater. Appl.* **2021**, *36*, 297.
[24] P. Widimsky, L. N. Hopkins, *Eur. Heart J.* **2016**, *37*, 3081.
[25] A. Ding, A. Braschkat, A. Guber, G. Cattaneo, *Clin. Neuroradiol.* **2021**, *31*, 671.
[26] G. F. M. Cattaneo, A. Ding, T. Jost, D. Ley, R. Mühl-Bennighaus, U. Yilmaz, H. Körner, W. Reith, A. Simgen, *Neuroradiology* **2017**, *59*, 1275.

[27] K. Gester, I. Lüchtefeld, M. Büsen, S. J. Sonntag, T. Linde, U. Steinseifer, G. Cattaneo, *Am. J. Neuroradiol.* **2016**, *37*, 490.
[28] G. Cattaneo, C. Bräuner, G. Siekmeyer, A. Ding, S. Bauer, M. Wohlschlögel, L. Lang, T. Hierlemann, M. Akimov, C. Schlensak, A. Schüßler, H. P. Wendel, S. Krajewski, *J. Mater. Sci. Mater. Med.* **2019**, *30*, 67.
[29] A. Link, T. Michel, M. Schaller, T. Tronser, S. Krajewski, G. Cattaneo, *Biomed. Mater.* **2021**, *16*, 015026.
[30] M. S. Y. Ng, J. Y. Suen, J. P. Tung, J. F. Fraser, *Haematologica* **2019**, *104*, 428.
[31] B. Huber, S. Engelhardt, W. Meyer, H. Krüger, A. Wenz, V. Schönhaar, G. Tovar, P. Kluger, K. Borchers, *J. Funct. Biomater.* **2016**, *7*, 11.
[32] J. Weber, M. Weber, A. Feile, C. Schlensak, M. Avci-Adali, *Cells* **2023**, *12*, 1217.
[33] A. McCulloch, A. Turcott, G. Graham, S. Frenklakh, K. O. Cardinal, *J. Neurointerv. Surg.* **2021**, *13*, 727.
[34] A. McCulloch, B. Yang, S. Frenklakh, P. Sah, K. O. Cardinal, *Neuroradiology* **2023**, *65*, 1507.
[35] B. Krüger-Genge, J. Franke, *Int. J. Mol. Sci.* **2019**, *20*, 4411.
[36] X. Ren, Y. Feng, J. Guo, H. Wang, Q. Li, J. Yang, X. Hao, J. Lv, N. Ma, W. Li, *Chem. Soc. Rev.* **2015**, *44*, 5680.
[37] M. A. Punchard, E. D. O'Cearbhaill, J. N. Mackle, P. E. McHugh, T. J. Smith, C. Stenson-Cox, V. Barron, *Ann. Biomed. Eng.* **2009**, *37*, 1322.
[38] R. N. Ghriallais, L. McNamara, M. Bruzzi, *J. R. Soc. Interface* **2013**, *10*, 20120965.
[39] I. S. Kinstlinger, G. A. Calderon, M. K. Royse, A. K. Means, B. Grigoryan, J. S. Miller, *Nat. Protoc.* **2021**, *16*, 3089.
[40] E. E. Antoine, F. P. Cornat, A. I. Barakat, *J. R. Soc. Interface* **2016**, *13*, 20160834.
[41] T. Tanaka, N. Hattori-Aramaki, A. Sunohara, K. Okabe, Y. Sakamoto, H. Ochiai, R. Hayashi, K. Kishi, *Int. J. Tissue Eng.* **2014**, *2014*, 621529.
[42] B. Liu, M. J. Qu, K. R. Qin, H. Li, Z. K. Li, B. R. Shen, Z. L. Jiang, *Biophys. J.* **2008**, *94*, 1497.
[43] T. Fee, S. Surianarayanan, C. Downs, Y. Zhou, J. Berry, *PLoS One* **2016**, *11*, e0154806.
[44] A. Salehi, S. Sprejz, H. Ruehl, M. Olayioye, G. Cattaneo, *J. Biomater. Sci. Polym. Ed.* **2024**, *35*, 1214.
[45] G. R. Liguori, B. F. Jeronimus, T. T. de Aquinas Liguori, L. F. P. Moreira, M. C. Harmsen, *Tissue Eng. Part C Methods* **2017**, *23*, 850.
[46] C. Liu, M. Pei, Q. Li, Y. Zhang, *Front. Med.* **2022**, *16*, 56.
[47] J. Liao, B. Xu, R. Zhang, Y. Fan, H. Xie, X. Li, *J. Mater. Chem. B* **2020**, *8*, 10023.
[48] K. Las Heras, M. Igartua, E. Santos-Vizcaino, R. M. Hernandez, *J. Controlled Release* **2020**, *328*, 532.
[49] Y. Zhu, Q. Zhang, S. Wang, J. Zhang, S. Fan, X. Lin, *Front. Bioeng. Biotechnol.* **2021**, *9*, 712262.
[50] J. R. Gershlak, S. Hernandez, G. Fontana, L. R. Perreault, K. J. Hansen, S. A. Larson, B. Y. K. Binder, D. M. Dolivo, T. Yang, T. Dominko, M. W. Rolle, P. J. Weathers, F. Medina-Bolivar, C. L. Cramer, W. L. Murphy, G. R. Gaudette, *Biomaterials* **2017**, *125*, 13.
[51] H. B. M. Lenting, M. M. C. G. Warmoeskerken, *J. Biotechnol.* **2001**, *89*, 217.
[52] M. Jorfi, E. J. Foster, *J. Appl. Polym. Sci.* **2015**, *132*, 41719.
[53] A. Golchin, T. Z. Farahany, *Stem Cell Rev. Rep.* **2019**, *15*, 166.
[54] R. Naomi, R. Bt Hj Idrus, M. B. Fauzi, *Int. J. Environ. Res. Public Health* **2020**, *17*, 6803.
[55] D. Fusco, F. Meissner, B. K. Podesser, A. Marsano, M. Grapow, F. Eckstein, B. Winkler, *Front. Cardiovasc. Med.* **2022**, *9*, 881557.
[56] C. Woffindin, N. A. Hoenich, J. N. S. Matthews, *Nephrol., Dial., Transplant.* **1992**, *7*, 340.
[57] D. J. Modulevsky, C. Lefebvre, K. Haase, Z. Al-Rekabi, A. E. Pelling, *PLoS One* **2014**, *9*, 0097835.
[58] M. Cevik, S. Dikici, *Soft Matter* **2024**, *20*, 338.
[59] J. K. R. Mutra, S. E. Jujjavarapu, N. Verma, *ACS Sustainable Chem. Eng.* **2023**, *11*, 6485.
[60] S. Dikici, Ç. Çavdaroğlu, *J. Mater. Sci.* **2023**, *58*, 16428.
[61] J. Yun, S. Robertson, C. Kim, M. Suzuki, W. L. Murphy, P. Gopalan, *Acta Biomater.* **2023**, *171*, 327.
[62] A. Salehi, M. A. Mobarhan, J. Mohammadi, H. Shahsavarani, M. A. Shokrgozar, A. Alipour, *J. Drug Delivery Sci. Technol.* **2021**, *63*, 102453.
[63] H. Bai, B. Xie, Z. Wang, M. Li, P. Sun, S. Wei, W. Wang, H. Wu, L. Bai, J. Li, *ACS Omega* **2021**, *6*, 11595.
[64] D. J. Modulevsky, C. M. Cuerrier, M. Leblanc-Latour, R. J. Hickey, R. J. K. Obhi, I. Shore, A. Galuta, K. L. A. Walker, E. C. Tsai, A. E. Pelling, BioRXiv, **2020**, 10.21.347807, https://doi.org/10.1101/2020.10.21.347807.
[65] A. L. Predeina, A. Y. Prilepskii, V. De Zea Bermudez, V. V. Vinogradov, *Nano Lett.* **2021**, *21*, 9853.
[66] B. Xie, X. Bai, P. Sun, L. Zhang, S. Wei, H. Bai, *Front. Bioeng. Biotechnol.* **2021**, *9*, 742285 .
[67] A. Salehi, M. A. Mobarhan, J. Mohammadi, H. Shahsavarani, M. A. Shokrgozar, A. Alipour, *Gene* **2020**, *757*, 144852.
[68] A. Salehi, M. A. Mobarhan, J. Mohammadi, H. Shahsavarani, M. A. Shokrgozar, A. Alipour, *J. Cell. Physiol.* **2021**, *236*, 5306.
[69] G. Fontana, J. Gershlak, M. Adamski, J. S. Lee, S. Matsumoto, H. D. Le, B. Binder, J. Wirth, G. Gaudette, W. L. Murphy, *Adv. Healthcare Mater.* **2017**, *6*, 1601225.
[70] S. Dikici, F. Claeyssens, S. MacNeil, *J. Biomater. Appl.* **2019**, *34*, 546.
[71] M. Toker, S. Rostami, M. Kesici, O. Gul, O. Kocaturk, S. Odabas, B. Garipcan, *Cellulose* **2020**, *27*, 7331.
[72] A. Sh, C. C. Mohan, U. PS, A. G. Krishnan, M. B. Nair, *Mater. Sci. Eng. C* **2021**, *119*, 111500.
[73] J. Lee, H. Jung, N. Park, S. H. Park, J. H. Ju, *Sci. Rep.* **2019**, *9*, 20194.
[74] J. Lacombe, A. F. Harris, R. Zenhausern, S. Karsunsky, F. Zenhausern, *Front. Bioeng. Biotechnol.* **2020**, *8*, 00932.
[75] R. J. Hickey, D. J. Modulevsky, C. M. Cuerrier, A. E. Pelling, *ACS Biomater. Sci. Eng.* **2018**, *4*, 3726.
[76] M. Leblanc Latour, M. Tarar, R. J. Hickey, C. M. Cuerrier, I. Catelas, A. E. Pelling, BioRXiv, **2020**, 01.15.906677, https://doi.org/10.1101/2020.01.15.906677.
[77] E. R. Robbins, G. D. Pins, M. A. Laflamme, G. R. Gaudette, *J. Biomed. Mater. Res. A* **2020**, *108*, 2123.
[78] K. B. Narayanan, R. Bhaskar, H. Kim, H. S. S. In, *Sustainability* **2023**, *15*, 15618.
[79] K. Driscoll, M. S. Butani, K. A. Gultian, A. McSweeny, J. M. Patel, S. L. Vega, *Cell Mol. Bioeng.* **2022**, *15*, 439.
[80] D. J. Modulevsky, C. M. Cuerrier, A. E. Pelling, *PLoS One* **2016**, *11*, e0157894.
[81] S. Walawalkar, S. Almelkar, *J. Biomater. Appl.* **2021**, *36*, 165.
[82] Y. Filiz, Y. Arslan, E. Duran, P. Saglam-Metiner, S. Horozoglu, A. Paradiso, D. C. Martinez, M. Sabour-Takanlou, M. Heljak, J. Jaroszewicz, C. Biray-Avci, W. Swieszkowski, O. Yesil-Celiktas, *Appl Mater Today* **2024**, *36*, 102015.
[83] J. Chakraborty, S. Roy, S. Ghosh, *Biomater. Sci.* **2020**, *8*, 1194.
[84] F. H. Silver, P. B. Snowhill, D. J. Foran, *Ann. Biomed. Eng.* **2003**, *31*, 793.
[85] E. VanBavel, P. Siersma, J. A. E. Spaan, *Am. J. Physiol., Heart Circ. Physiol.* **2003**, *285*, H1986.
[86] X. Zhang, R. R. Kinnick, M. Fatemi, J. F. Greenleaf, *IEEE Trans. Ultrason. Ferroelectr. Freq. Control* **2005**, *52*, H1986642.
[87] F. H. Silver, *Online J. Cardiol. Res. Rep.* **2021**, *31*, 793.
[88] J. Cheng, C. Wang, Y. Gu, *Biomed. Mater. Eng.* **2019**, *30*, 191.
[89] Y. Yokota, Y. Kawamura, F. Nogata, H. Morita, Y. Uno, T. Kawamura, N. Hotta, IFMBE World Congress on Medical Physics and Biomedical Engineering, Springer, Berlin/Heidelberg **2009**, p. 1226, https://doi.org/10.1007/978-3-642-03882-2_325.

[90] R. K. V., N. P. M., J. Joseph, M. I. Shah, M. Sivaprakasam, 2018 IEEE International Symposium on Medical Measurements and Applications (MeMeA), Rome, Italy, June **2018**. pp. 1–6, https://doi.org/10.1109/MeMeA.2018.8438729.
[91] C. J. van Andel, P. V. Pistecky, C. Borst, *Ann. Thorac. Surg.* **2003**, *76*, 58.
[92] M. B. Elliott, B. Ginn, T. Fukunishi, D. Bedja, A. Suresh, T. Chen, T. Inoue, H. C. Dietz, L. Santhanam, H. Q. Mao, N. Hibino, S. Gerecht, *Proc. Natl. Acad. Sci. U. S. A.* **2019**, *116*, 12710.
[93] P. Gupta, K. L. Lorentz, D. G. Haskett, E. M. Cunnane, A. K. Ramaswamy, J. S. Weinbaum, D. A. Vorp, B. B. Mandal, *Acta Biomater.* **2020**, *105*, 146.
[94] C. Yu, S. Sharma, C. H. Fang, H. Jeong, J. Li, G. Joice, T. J. Bivalacqua, A. Singh, *ACS Appl. Bio Mater.* **2020**, *3*, 1331.
[95] S. Wang, Y. Zhang, H. Wang, G. Yin, Z. Dong, *Biomacromolecules* **2009**, *10*, 2240.
[96] J. M. Caves, V. A. Kumar, A. W. Martinez, J. Kim, C. M. Ripberger, C. A. Haller, E. L. Chaikof, *Biomaterials* **2010**, *31*, 7175.
[97] K. Billiar, J. Murray, D. Laude, G. Abraham, N. Bachrach, *J. Biomed. Mater. Res.* **2001**, *56*, 101.
[98] T. P. Lemmens, V. Bröker, M. Rijpkema, C. C. W. Hughes, L. J. Schurgers, J. M. E. M. Cosemans, *Thromb. Res.* **2024**, *236*, 179.
[99] J. Táborská, Z. Riedelová, E. Brynda, P. Májek, T. Riedel, *RSC Adv.* **2021**, *11*, 5903.
[100] K. A. Sindhu, R. Prasanth, V. K. Thakur, in *Nanocellulose Polymer Nanocomposites*, Wiley, New York/Chichester, UK, **2014**. pp. 437–77.
[101] D. Tomaszewski, J. Zieliński, *Flora – Morphol., Distribut., Funct. Ecol. Plants* **2014**, *209*, 215.
[102] S. J. Liliensiek, P. Nealey, C. J. Murphy, *Tissue Eng Part A* **2009**, *15*, 2643.
[103] S. Brody, T. Anilkumar, S. Liliensiek, J. A. Last, C. J. Murphy, A. Pandit, *Tissue Eng.* **2006**, *12*, 413.
[104] H. E. Burton, R. Cullinan, K. Jiang, D. M. Espino, *R. Soc. Open Sci.* **2019**, *6*, 190915.
[105] Y. Li, Y. Fu, H. Zhang, X. Wang, T. Chen, Y. Wu, X. Xu, S. Yang, P. Ji, J. Song, *Adv. Healthcare Mater.* **2022**, *11*.
[106] S. J. Allan, M. J. Ellis, P. A. De Bank, *J. Biomed. Mater. Res. A* **2021**, *109*, 2471.
[107] Y. W. Cheng, D. J. Shiwarski, R. L. Ball, K. A. Whitehead, A. W. Feinberg, *ACS Biomater. Sci. Eng.* **2020**, *6*, 3046.
[108] J. Gerdes, H. Lemke, H. Baisch, H. H. Wacker, U. Schwab, H. Stein, *J. Immunol.* **1984**, *133*, 1710.
[109] J. Bullwinkel, B. Baron-Lühr, A. Lüdemann, C. Wohlenberg, J. Gerdes, T. Scholzen, *J. Cell. Physiol.* **2006**, *206*, 624.
[110] Y. T. Yeh, S. S. Hur, J. Chang, K. C. Wang, J. J. Chiu, Y. S. Li, S. Chien, *PLoS One* **2012**, *7*, e46889.
[111] B. C. Heng, P. P. Bezerra, Q. R. Meng, D. W. L. Chin, L. B. Koh, H. Li, H. Zhang, P. R. Preiser, F. Y. C. Boey, S. S. Venkatraman, *Biointerphases* **2010**, *5*, FA53.
[112] F. E. Rodger, F. M. Young, H. M. Fraser, P. J. Illingworth, *Human Reprod.* **1997**, *12*, 1723.
[113] R. Stănescu, A. C. Didilescu, A. M. Jianu, M. C. Rusu, *Rom. J. Morphol. Embryol.* **2012**, *53*, 375.
[114] M. Krstulja, D. Bonifacic, S. Cvejanović, *Open Life Sci.* **2008**, *3*, 113.
[115] A. Pappalardo, L. Herron, D. E. Alvarez Cespedes, H. E. Abaci, *Adv. Wound Care* **2021**, *10*, 490.
[116] M. Sgarioto, P. Vigneron, J. Patterson, F. Malherbe, M. D. Nagel, C. Egles, *C R Biol.* **2012**, *335*, 520.
[117] J. Furuzawa-Carballeda, O. A. Muñoz-Chablé, J. Barrios-Payán, R. Hernández-Pando, *Eur. J. Clin. Invest.* **2009**, *39*, 591.
[118] E. McLucas, M. T. Moran, Y. Rochev, W. M. Carroll, T. J. Smith, *Endothelium* **2006**, *13*, 35.
[119] N. An, A. Schedle, M. Wieland, O. Andrukhov, M. Matejka, X. Rausch-Fan, *J. Biomed. Mater. Res. A* **2010**, *93A*, 364.
[120] K. Zhou, Y. Li, L. Zhang, L. Jin, F. Yuan, J. Tan, G. Yuan, J. Pei, *Bioact. Mater.* **2021**, *6*, 262.
[121] T. W. Chung, D. Z. Liu, S. Y. Wang, S. S. Wang, *Biomaterials* **2003**, *24*, 4655.
[122] Y. Shen, G. Wang, L. Chen, H. Li, P. Yu, M. Bai, Q. Zhang, J. Lee, Q. Yu, *Acta Biomater.* **2009**, *5*, 3593.
[123] B. Yi, Q. Xu, W. Liu, *Bioact. Mater.* **2022**, *15*, 82.
[124] D. Bhattacharyya, H. Xu, R. R. Deshmukh, R. B. Timmons, K. T. Nguyen, *J. Biomed. Mater. Res. A* **2010**, *94A*, 640.
[125] R. D. Chavez, S. L. Walls, K. O. Cardinal, *PLoS One* **2019**, *14*, 0217709.
[126] N. Zebda, O. Dubrovskyi, K. G. Birukov, *Microvasc. Res.* **2012**, *83*, 71.
[127] W. H. Ziegler, R. C. Liddington, D. R. Critchley, *Trends Cell Biol.* **2006**, *16*, 453.
[128] L. Indolfi, A. B. Baker, E. R. Edelman, *Biomaterials* **2012**, *33*, 7019.
[129] E. Dejana, D. Vestweber, *Prog. Mol. Biol. Transl. Sci.* **2013**, *116*, 119.
[130] K. Tsuji-Tamura, M. Ogawa, *Inflamm. Regen.* **2018**, *38*, 25.
[131] Y. S. J. Li, J. H. Haga, S. Chien, *J. Biomech.* **2005**, *38*, 1949.
[132] L. Soletti, Y. Hong, J. Guan, J. J. Stankus, M. S. El-Kurdi, W. R. Wagner, D. A. Vorp, *Acta Biomater.* **2010**, *6*, 110.